PCP
PLANT & CELL PHYSIOLOGY

Regular Paper

Identification of Phosphoinositide-Binding Protein PATELLIN2 as a Substrate of Arabidopsis MPK4 MAP Kinase during Septum Formation in Cytokinesis

Takamasa Suzuki[1,2,3,6], Chiyuki Matsushima[2], Shingo Nishimura[1], Tetsuya Higashiyama[1,3,4], Michiko Sasabe[5] and Yasunori Machida[1,*]

[1]Division of Biological Sciences, Graduate School of Science, Nagoya University, Furo-cho, Chikusa-ku, Nagoya, 464-8602 Japan
[2]Graduate School of Bioagricultural Sciences, Nagoya University, Furo-cho, Chikusa-ku, Nagoya, 464-8601 Japan
[3]JST, ERATO, Higashiyama Live-Holonics Project, Nagoya University, Furo-cho, Chikusa-ku, Nagoya, 464-8602 Japan
[4]Institute of Transformative Bio-Molecules, Nagoya University, Furo-cho, Chikusa-ku, Nagoya, 464-8602 Japan
[5]Department of Biology, Faculty of Agriculture and Life Science, Hirosaki University, 3 Bunkyo-cho, Hirosaki, 036-8561 Japan
[6]Present address: College of Bioscience and Biotechnology, Chubu University, 1200 Matsumoto-cho, Kasugai, Aichi 487-8501 Japan.
*Corresponding author: E-mail, yas@bio.nagoya-u.ac.jp; Fax, +81-52-789-2966.
(Received October 7, 2015; Accepted May 5, 2016)

The phosphorylation of proteins by protein kinases controls many cellular and physiological processes, which include intracellular signal transduction. However, the underlying molecular mechanisms of such controls and numerous substrates of protein kinases remain to be characterized. The mitogen-activated protein kinase (MAPK) cascade is of particular importance in a variety of extracellular and intracellular signaling processes. In plant cells, the progression of cytokinesis is an excellent example of an intracellular phenomenon that requires the MAPK cascade. However, the way in which MAPKs control downstream processes during cytokinesis in plant cells remains to be fully determined. We show here that comparisons, by two-dimensional difference gel electrophoresis, of phosphorylated proteins from wild-type *Arabidopsis thaliana* and mutant plants defective in a MAPK cascade allow identification of substrates of a specific MAPK. Using this method, we identified the PATELLIN2 (PATL2) protein, which has a SEC14 domain, as a substrate of MPK4 MAP kinase. PATL2 was concentrated at the cell division plane, as is MPK4, and had binding affinity for phosphoinositides. This binding affinity was altered after phosphorylation of PATL2 by MPK4, suggesting a role for the MAPK cascade in the formation of cell plates via regeneration of membranes during cytokinesis.

Keywords: Cytokinesis • MAP kinase • Membrane protein PATL2 • Phosphoinositide-binding protein • Phosphoproteomics • SEC14–GOLD domain.

Abbreviations: CDK, cyclin-dependent kinase; DIC, differential interference contrast; 2D-DIGE, two-dimensional difference gel electrophoresis; G3GFP, G3 green fluorescent protein; GFP, green fluorescent protein; GST, glutathione *S*-transferase; MALDI-TOF/MS, matrix-assisted laser desorption ionization time-of-flight mass spectrometry; MT, microtubule; MAP65, microtubule-associated protein 65; MAPK, mitogen-activated protein kinase; MBP, maltose-binding protein; mRFP, monomeric red fluorescent protein; NACK1, NPK1-activating kinesin-like protein 1; NPK1, nucleus- and phragmoplast-localized protein kinase 1; PATL, patellin; PPase, phosphatase; PI, phosphatidylinositol; PI3P, phosphatidylinositol 3-phosphate; PI4P, phosphatidylinositol 4-phosphate; PI5P, phosphatidylinositol 5-phosphate; $PI(3,4)P_2$, phosphatidylinositol 3,4-bisphosphate; $PI(3,5)P_2$, phosphatidylinositol 3,5-bisphosphate; $PI(4,5)P_2$, phosphatidylinositol 4,5-bisphosphate; $PI(3,4,5)P_3$, phosphatidylinositol 3,4,5-trisphosphate; RT–PCR, reverse transcription–PCR.

Introduction

Mitogen-activated protein kinase (MAPK) cascades play a central role in numerous extracellular and intracellular signaling processes that co-ordinately regulate gene expression, mitosis, metabolism, motility, survival, apoptosis, defense and differentiation (Nakagami et al. 2005, Cargnello and Roux. 2011, Yang et al. 2013, Meng and Zhang 2013). A typical cascade is composed of members of three classes of kinases, namely a MAP kinase (MAPK), a MAPK kinase (MAPKK) and a MAPKK kinase (MAPKKK). Each MAPKKK phosphorylates a MAPKK to activate it. In turn, the MAPKK phosphorylates a MAPK to activate this latter enzyme. Cell division in eukaryotes is controlled by MAPK cascades at several critical junctures, e.g. entry into the cell cycle; transition from the G_2 phase to the M phase; and, in yeast and animal cells, at the spindle assembly checkpoint (Widmann et al. 1999, Chang and Karin 2001). The progression of cytokinesis of plant cells, in particular, is also influenced by a MAPK cascade (Nishihama and Machida 2001, Suzuki and Machida 2008, Sasabe and Machida 2012, Sasabe and Machida 2014).

Plant cytokinesis is achieved via the formation of a septum that is called the cell plate, and formation of the cell plate is mediated by the co-ordinated turnover of microtubules (MTs) and the synthesis of cell membranes and cell walls (Heese et al. 1998, Otegui and Staehelin 2000, Otegui et al. 2005, Murata et al. 2013). The formation and development of the cell plate

Plant Cell Physiol. 57(8): 1744–1755 (2016) doi:10.1093/pcp/pcw098, Advance Access publication on 19 May 2016, available online at www.pcp.oxfordjournals.org

occurs in a plant-specific apparatus called the phragmoplast (Sasabe and Machida 2014). Components of the cell plate are transported along MTs by vesicles derived from Golgi bodies. The endocytic delivery of cell surface materials also contributes to the formation of the cell plate (Boutté et al. 2010, Frescatada-Rosa et al. 2014). Vesicles containing materials for the construction of new plasma membranes and cell walls accumulate at the cell plate and fuse to the pre-existing immature cell plate, with resultant expansion of the cell plate.

In tobacco cells, a MAPK cascade, consisting of nucleus- and phragmoplast-localized protein kinase 1 (NPK1) MAPKKK, NQK1 MAPKK and NRK1 MAPK, regulates cytokinesis (Nishihama et al. 2001, Soyano et al. 2003). NPK1 is activated by binding to NPK1-activating kinesin-like protein 1 (NACK1; Ishikawa et al. 2002, Nishihama et al. 2002, Naito and Goshima 2015, Sasabe et al. 2015), and the activity of the complex is negatively regulated by phosphorylation of both NPK1 and NACK1 by cyclin-dependent kinase (CDK) (Sasabe et al. 2011a). The NACK1-regulated system, including the MAPK cascade, has been designated the NACK–PQR pathway (Soyano et al. 2003). The NACK–PQR pathway is conserved in *Arabidopsis thaliana*, as shown in **Fig. 1A**. The *AtNACK1/HINKEL*, *MAPKK 6* (*MKK6*)/*ANQ* and *MAPK 4* (*MPK4*) genes are the orthologs in *A. thaliana* of *NACK1*, *NQK1* (encoding MAPKK) and *NRK1* (encoding MAPK) of tobacco, respectively (Nishihama et al. 2002, Strompen et al. 2002, Kosetsu et al. 2010, Takahashi et al. 2010). In *A. thaliana*, the components of the NACK–PQR pathway are concentrated at the plane of cell division in the phragmoplast and are required for cytokinesis (Tanaka et al. 2004). MPK4 MAP kinase is required not only for mitosis but also for meiosis (Zeng et al. 2011).

Details of the control by the NACK–PQR pathway of downstream processes during progression of the cell cycle in plant cells remain to be clarified. Members of the microtubule-associated protein 65 family, namely, MAP65-1 in tobacco and MAP65-1, MAP65-2 and MAP65-3 in *A. thaliana*, have been identified as targets of NRK1 (Sasabe et al. 2006) and MPK4 MAP kinases in the respective plants (Beck et al. 2010, Kosetsu et al. 2010, Sasabe et al. 2011b). It has also been reported that MPK6 contributes to shoot apical meristem homeostasis (Betsuyaku et al. 2011) and stomatal development (Lampard et al. 2008, Serna 2014) in *A. thaliana*. A role for MPK4 in the

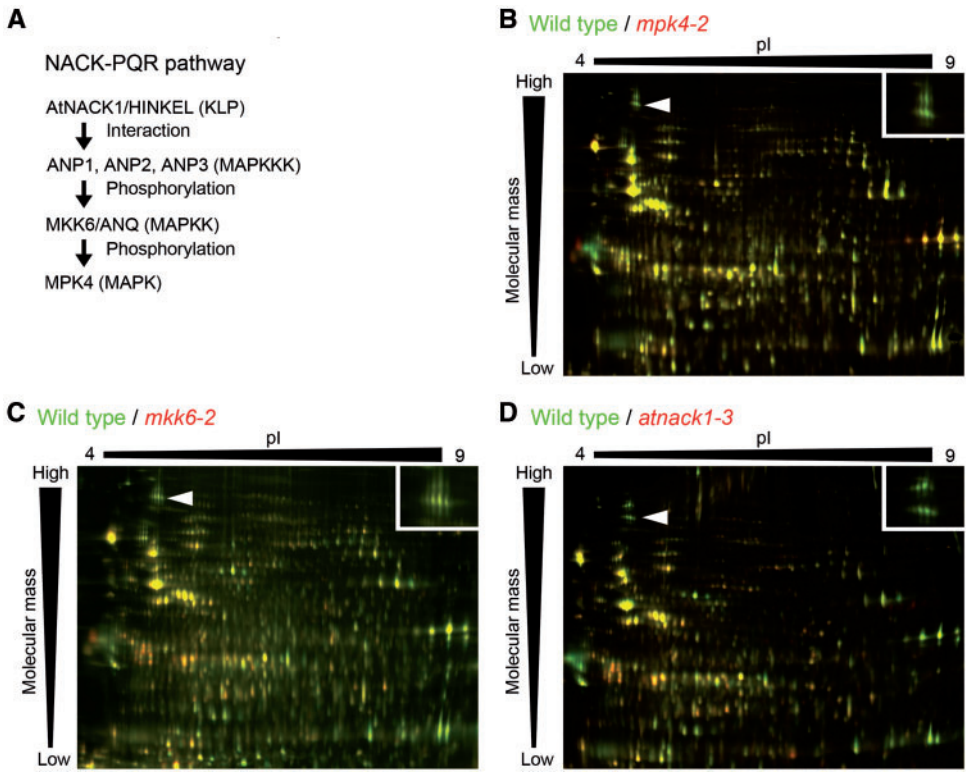

Fig. 1 Screening for targets of MPK4 by 2D-DIGE. (A) The NACK–PQR pathway in *A. thaliana*. KLP, kinesin-like protein. (B) A representative comparison of phosphorylated proteins from the wild type with those from the *mpk4-2* mutant by 2D-DIGE. Phosphorylated proteins prepared from wild-type and *mpk4-2* roots were labeled with the fluorophores Cy5 and Cy3, respectively, Then labeled proteins were mixed and the mixture was subjected to 2D-DIGE. Signals due to Cy5 and Cy3 were visualized separately as green and red spots, respectively. Images obtained from the wild type (green) and the *mpk4-2* mutant (red) were merged. Spots corresponding to PATL2 proteins are indicated by an arrowhead, and an enlarged image of these spots is shown in the inset. (C) Proteins from wild-type and *mkk6-2/anq1-2* plants were labeled with the fluorophores Cy2 and Cy5, respectively. After 2D-DIGE, signals due to Cy2 and Cy5 were visualized separately as green and red spots, respectively, and then images were merged. Arrowheads and insets are shown similarly to those in (B). (D) Proteins from wild-type and *atnack1-3* plants were labeled with Cy2 and Cy3, respectively. After 2D-DIGE, signals due to Cy2 and Cy3 were visualized separately as green and red spots, respectively, and then images were merged. Arrowheads and insets are shown similarly to those in (B).

plant immune systems has also been suggested (Petersen et al. 2000, Kong et al. 2012, Zhang et al. 2012, Meng and Zhang 2013). It is now necessary to identify the target proteins of MAPKs if we are to unravel the regulatory systems that are controlled by these MAPKs. Two-dimensional differential gel electrophoresis (2D-DIGE) of phosphoproteins has been developed as a method which is studied for the identification of potential target proteins of kinases (Ueda et al. 2004, Tang et al. 2008). In the present study, we used 2D-DIGE to compare phosphorylated proteins from plants with mutations in components of the NACK–PQR pathway of *A. thaliana*, and our observations allowed us to identify a new target of MAPK4.

Results

Identification of substrates of MPK4 MAP kinase by 2D-DIGE

To identify substrates of MPK4 in vivo, we used 2D-DIGE to compare phosphorylated proteins from the wild type with those from mutants (*mpk4-2*, *mkk6-2/anq1-2* and *atnack1-3*) that were defective in the NACK–PQR pathway (**Fig. 1**). Proteins extracted from tissue of the wild type and these mutant plants were subjected to further treatment to concentrate the phosphorylated proteins, as described in the Materials and Methods. Analysis by SDS–PAGE of the resultant phosphorylated protein fractions confirmed significant enrichment for these proteins (**Supplementary Fig. S1**). Phosphorylated proteins from wild-type and mutant plants were covalently labeled with different respective fluorophores. Then the labeled proteins from the two sources were combined and the proteins were subjected to 2D-DIGE. After separation of the combined proteins by 2D-PAGE, phosphoproteins derived from wild-type plants were visualized as green spots, while those derived from the mutants were red, and both images were merged. If, in a particular spot, the amount of a certain phosphorylated protein from the wild type was present at the same level as that from the mutant, the spot appeared yellow. A spot with a lower amount of a particular phosphorylated protein from the mutant plant, as compared with that from the wild-type plant should appear greener. Almost all spots containing proteins from wild-type and *mpk4-2* plants were yellow (**Fig. 1B**), indicating that these spots contained similar amounts of the respective phosphorylated proteins derived from both wild-type and *mpk4-2* plants. However, there were several green spots, which appeared to represent candidate targets of MPK4. We performed similar analyses with *mkk6-2/anq-2* and *atnack1-3* mutant plants and, again, we observed several distinct green spots in each case (**Fig. 1C, D**). Several contiguous spots (e.g. spots indicated by arrowheads in **Fig. 1B–D**) were always green in all images obtained from the analysis of the three different mutants, suggesting that proteins in these spots were likely targets of phosphorylation in the NACK–PQR pathway.

To identitfy the candidate proteins, we cut out portions of the above-mentioned gels that contained the spots of interest and digested the proteins in the gel with trypsin. The mass of each peptide was determined by matrix-assisted laser desorption ionization time-of-flight mass spectrometry (MALDI-TOF/MS), and the mass spectra obtained were used to identify the corresponding proteins by peptide mass fingerprinting. Several contiguous spots, in a pattern that we observed on all our 2D-DIGE gels (e.g. **Fig. 1B**–1D, arrowheads), corresponded to the protein Patellin2 (PATL2: AT1G22530; **Fig. 2A**), which is a plant SEC14-like protein (Peterman et al. 2004). The sequence coverage of authentic PATL2 by the peptides in the present study was 24%. This low coverage might have been due to the acidic region in the N-terminal half of the amino acid sequence of authentic PATL2. The majority of the peptides identified by MALDI-TOF/MS originated from the C-terminal half of PATL2 (**Fig. 2A**). The calculated molecular mass and pI of PATL2 are 76 kDa and 4.6, respectively.

We carried out 2D-DIGE analysis of phosphorylated proteins extracted from wild-type and *patl2-3* mutant plants (**Fig. 2B**). Using antibodies specific for the the synthetic peptide of PATL2 (residues 399–411), Western blot analysis of protein extracts

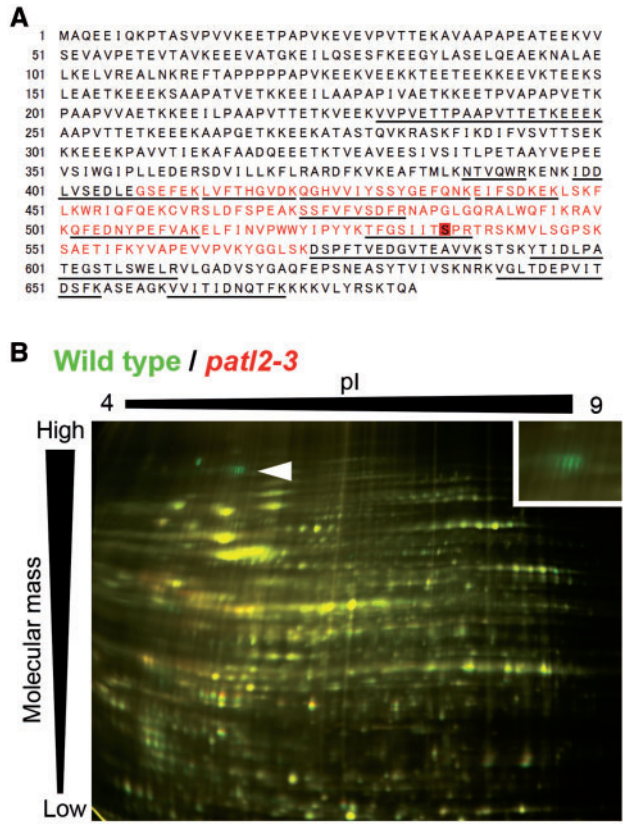

Fig. 2 Identification of PATL2 by MALDI-TOF/MS. (A) The predicted amino acid sequence of PATL2 from *A. thaliana*. The peptide fragments detected by MALDI-TOF/MS in the present study are underlined. The SEC14 domain is indicated in red, and the phosphorylatable serine residue at positions 536 is shown in a red box. (B) The 2D-DIGE image of proteins from wild-type and *patl2-3* mutant plants. Proteins from wild-type and *patl2-3* plants were labeled with Cy2 and Cy5, respectively. Subsequent procedures were carried out as described in the legend to **Fig. 1C**. The arrowhead and inset are shown similarly to those in **Fig. 1**.

prepared from plants with three different *patl2* alleles, including *patl2-3*, showed that these mutants did not produce a protein that corresponded, in terms of molecular mass, to PATL2 (**Supplementary Fig. S2**). After 2D-DIGE analysis with the *patl2-3* mutant, the spots that we had identified putatively as PATL2 (as shown in **Fig. 1B–D**) again exhibited a green color, as shown in **Fig. 2B**, confirming that proteins recognized as green spots in **Fig. 1** corresponded to *PATL2*-derived proteins.

PATL2 is the closest protein to PATL1 in the proteome of *A. thaliana*, and both contain the SEC14 domain, which is ubiquitously conserved throughout the eukaryotic kingdom and has the ability to bind and transfer phospholipids (Mousley et al. 2007, Saito et al. 2007, Schaaf et al. 2008). Within the SEC14 domains of these PATL proteins, 88% of amino acid residues are identical (Peterman et al. 2004).

Expression of PATL2 was unaffected by mutations in genes for AtNACK1, MKK6 and MPK4

We compared the levels of PATL2 in mutants with defects in genes for AtNACK1, MKK6 and MPK4 in the NACK–PQR pathway with the levels in the wild-type siblings. Protein bands corresponding to levels of PATL2 in these mutants were of similar intensity (**Fig. 3A**), indicating that the mutations in the *AtNACK1*, *MKK6* and *MPK4* genes did not affect the amount of PATL2 protein produced. We also measured levels of PATL2 mRNA by real-time reverse transcription–PCR (RT–PCR) (**Fig. 3B**). There were no significant differences among the mutants and the wild-type siblings. Our results indicated that defects in genes for components of the NACK–PQR pathway reduced the relative amount of the phosphorylated form of PATL2 protein in the mutant lines.

Phosphorylation of PATL2 in vivo

To examine the phosphorylation of PATL2 in vivo, we fractionated proteins by 2D gel electrophoresis with subsequent immunoblotting (2D-Western blotting) with PATL2-specific antibodies. We incubated extracts of total protein from roots of wild-type plants with and without lambda protein phosphatase (λ PPase) and then subjected the extracts to 2D gel electrophoresis and immunoblotting (**Fig. 4A, B**). We observed three spots, designated 0, 1 and 2 (left panel of **Fig. 4A**), and determined the intensity of each spot (right panel of **Fig. 4A**). After treatment with λ PPase, the relative intensities of spots 1 and 2 were reduced, while that of spot 0 increased (**Fig. 4A, B**). These results imply that PATL2 might be phosphorylated in vivo, that the protein corresponding to spot 0 might contain no phosphate groups and that proteins in spots 1 and 2 might contain one and/or increasing numbers of phosphate groups.

We analyzed, similarly, the phosphorylation status of endogenous PATL2 in tissue of wild-type and *mpk4-2* mutant plants by 2D-Western blotting (**Fig. 4C, D**). In the analysis of the wild-type plant, the intensity of spot 1 was the highest among those of spots of phosphorylated PATL2 (**Fig. 4C**). However, the relative intensity of spot 0 was highest in the case of the *mpk4-2* mutant (**Fig. 4D**). These results suggested that the relative amount of the non-phosphorylated form of PATL2 was higher in the *mpk4-2* mutant than in the wild type and that MPK4 was responsible for phosphorylation of some part of the phosphorylation.

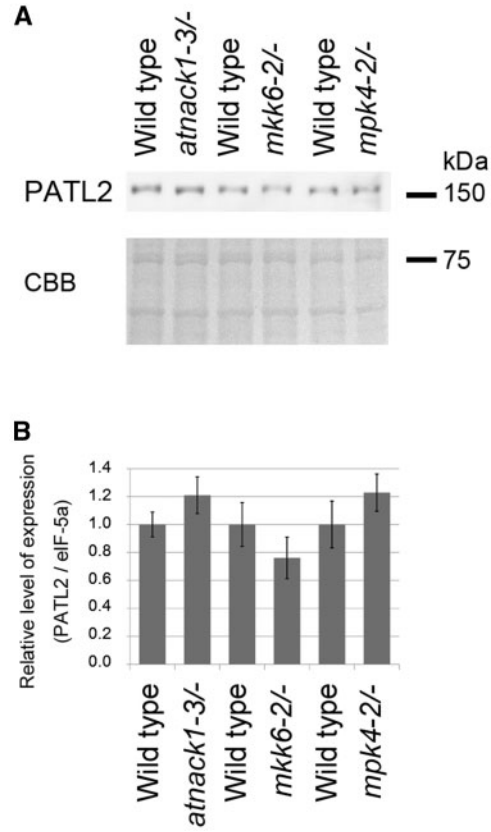

Fig. 3 Analysis of the expression of PATL2. (A) Total protein extracted from wild-type and mutant siblings was subjected to SDS–PAGE, and the PATL2 protein was detected with PATL2-specific antibodies (upper panel). The membrane was stained with Coomassie Brilliant Blue (CBB; lower panel). Note that the relative molecular mass of the detected band was larger than the estimated size of 76.0 kDa, maybe because of the presence of many acidic amino acid residues in the N-terminal half (pI = 4.6; see text). (B) Results of analysis by real-time RT–PCR of transcripts of the *PATL2* gene in wild-type and mutant siblings. Levels of *eIF5A* transcripts were used as a reference, and relative values refer to ratios calculated by dividing the level of expression in mutants by that in the wild type. The values shown represent averages ± SD of measurements of four independent experiments in each case. The value was normalized by reference to that for eIF5a transcripts.

MPK4 phosphorylates PATL2 in vitro

We examined the phosphorylation of PATL2 by MPK4 in vitro, using glutathione *S*-transferase-fused PATL2 (GST–PATL2) and histidine- and T7-tagged MPK4 (HisT7-MPK4) that had been produced in *Escherichia coli*. HisT7-MPK4 MAP kinase was activated by active NQK1 MAPKK. MPK4 phosphorylated GST–PATL2 (**Fig. 5A**). We identified six putative sites of phosphorylation of PATL2 by MPK4 (serine residues at positions 468, 536 and 575; and threonine residues at positions 20, 190 and 236), each of which is followed by the proline residue. We introduced mutations that replaced these serine and threonine residues with alanine residues. We first generated a pair of

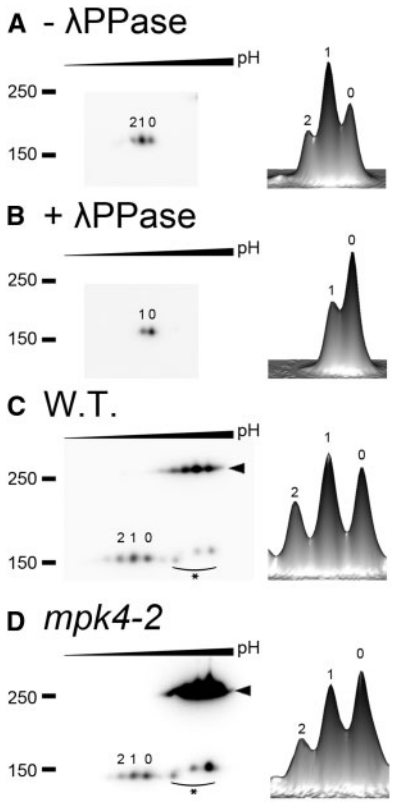

Fig. 4 2D-Western blotting for identification of phosphorylation of PATL2 in vivo. (A) Total proteins extracted from wild-type plants were separated by 2D gel electrophoresis and the PATL2 was detected with PATL2-specific antibodies (2D-Western blotting). The results of densitometric analysis are shown in the right-hand panel. (B) λ phosphatase-treated proteins were subjected to 2D-Western blotting. (C) Total protein from a wild-type plant was mixed with MBP–PATL2 protein, which had been generated in *E. coli* and was used as a marker for positioning on membranes, and the mixture was subjected to 2D-Western blotting. PATL2 was visualized as described above. Spots of MBP–PATL2 are indicated by arrowheads, and the regions into which its degradation products have spread are indicated by an arc with an asterisk. (D) Total proteins from an *mpk4-2* mutant plant were subjected similarly to 2D-Western blotting and PATL2 was visualized as described above.

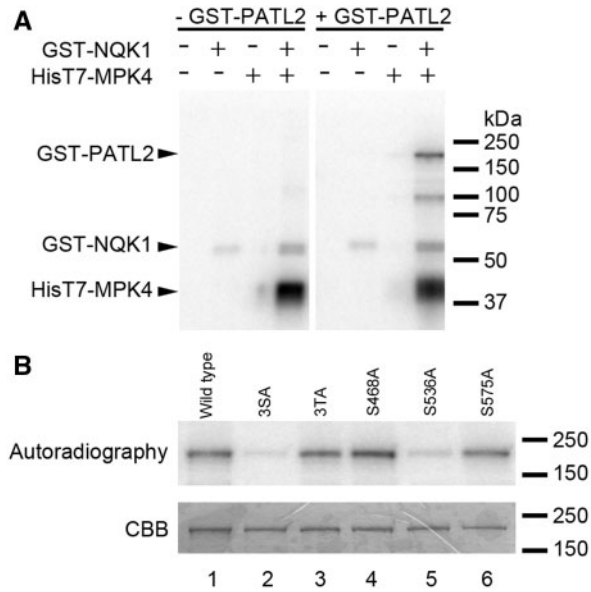

Fig. 5 Phosphorylation of PATL2 by MPK4 in vitro. (A) GST–PATL2 was incubated with or without HisT7-MPK4 and GST–NQK1 in the presence of [γ-^{32}P]ATP. After SDS–PAGE, phosphorylated GST–PATL2 was detected by autoradiography. Arrowheads indicate the positions of the three proteins. Note that the relative molecular mass of the detected band was larger than the estimated size of GST–PATL2 of 102 kDa as described in the legend of **Fig. 3**. (B) Kinase assays in vitro of GST–PATL2 and of the derivatives in which serine and threonine residues had been replaced by alanine residues. In the GST–PATL2 derivatives indicated as 3SA and 3TA, three serine residues and three threonine residues, respectively, were replaced by alanine residues (see text). S468A, S536A and S575A represent replacement of a serine residue at the indicated position by an alanine residue. Images after autoradiography (upper panel) and staining with Coomassie Brilliant Blue (CBB; lower panel) are shown.

mutants in which one member contained three alanine replacements at the serine residues (designated PATL2:3SA) and the other contained three alanine replacements at the threonine residues (designated PATL2:3TA). We examined whether the two mutant proteins could be phosphorylated by MPK4 in vitro (**Fig. 5B**). GST–PATL2:3SA was only very weakly phosphorylated by MPK4 (**Fig. 5B**, lane 2), suggesting that the three serine residues of PATL2 include a major site(s) of phosphorylation by MPK4. In contrast, GST–PATL2:3TA was efficiently phosphorylated by MPK4 (**Fig. 5B**, lane 3), and the replacements of the threonine residues by alanine had no effect on the extent of phosphorylation. Next, we replaced each of the three individual serine residues, separately, with alanine and repeated the kinase assays. The extent of phosphorylation by MPK4 was significantly reduced in the mutant protein with replacement of serine by alanine at position 536 (GST–PATL2:S536A; **Fig. 5B**, lane 5). Thus, the serine residue at position 536 of PATL2 appeared to be the major site of phosphorylation by MPK4.

PATL2 is concentrated at the newly synthesized cell plate

We examined the subcellular localization of PATL2 by expressing the recombinant gene for G3 green fluorescent protein-fused PATL2 (PATL2–G3GFP) in root cells of transgenic plants of *A. thaliana* under the control of the 35S promoter of *Cauliflower mosaic virus* (Kawakami and Watanabe 1997, for G3GFP, which has two amino acid replacements, of the Ser65 and Tyr145 with alanine and phenylalanine, respectively). We monitored the fluorescence of GFP in root tissue by confocal laser scanning microscopy (**Fig. 6**). We detected fluorescence due to PATL2–G3GFP mainly at the cell periphery, which suggested the presence of PATL2 at the plasma membrane or at the cell wall at the cell boundary. However, fluorescence due to PATL2–G3GFP was not uniformly distributed to all cell boundaries in the division zone: signals from the apical and basal (horizontal) planes of cell division were much stronger than those from the lateral (vertical) boundaries (**Fig. 6B**).

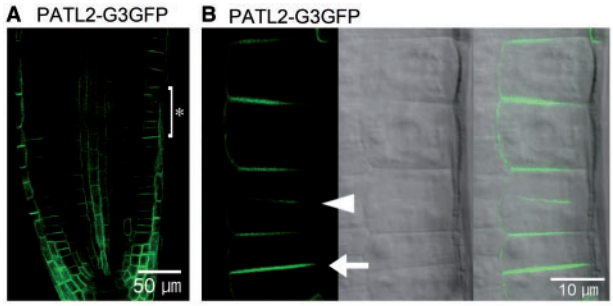

Fig. 6 Subcellular localization of PATL2 in root cells. (A) The root tip of a transformant of *A. thaliana* that expressed PATL2–G3GFP. (B) Magnified views of the region indicated by a bracket and an asterisk in (A). The arrow indicates the strongest signal, and the arrowhead indicates a developing cell plate. A fluorescent image due to PATL2–G3GFP, a differential interference contrast (DIC) image and a merged image are shown on the left, in the center and on the right, respectively.

Moreover, some apical and basal planes were associated with stronger signals than others, as indicated by the arrow in **Fig. 6B**. Stronger signals were typically found on the apical or basal planes of relatively small cells, suggesting that these planes had been newly synthesized in association with cell division. Signals due to PATL2–G3GFP were also evident at the premature cell plate, which appeared to be expanding during cytokinesis (arrowhead in **Fig. 6B**). These images suggested that PATL2 might be concentrated at the cell plate during the progression of cytokinesis and temporarily retained at the division plane even after the maturation of cell plates. The patterns that we observed were similar to those of PATL1, as revealed previously by immunostaining (Peterman et al. 2004). We also expressed PATL2–G3GFP with the S536A mutation in plants of *A. thaliana*, but found no obvious differences, in terms of the pattern of subcellular localization, from the pattern described above (data not shown). In addition, we also detected intense signals due to GFP over the entire cell periphery in the lateral root cap and on all division planes of cells in the central cylinder above the quiescent center (**Fig. 6A**).

To investigate a possible relationship between the dynamics of distribution of PATL2 and cytokinetic kinesin NACK1 in living cells, we introduced DNA constructs that encoded monomeric red fluorescent protein (mRFP; Campbell et al. 2002) and monomeric red fluorescent protein-fused PATL2 (mRFP–PATL2) separately into tobacco BY-2 cells. Most of the fluorescent signals due to mRFP–PATL2 were observed at the cell boundaries and at the cell plate (arrowhead in **Fig. 7A**), while fluorescence due to mRFP alone was distributed over the entire cytoplasm and nucleus, with the exception of vacuoles (**Fig. 7B**). Examination of plasmolyzed cells revealed that signals due to mRFP–PATL2 were concentrated at the plasma membrane, as opposed to the cell wall (**Fig. 7C, D**). Immunofluorescence staining of MTs confirmed that mRFP–PATL2 was concentrated at the equatorial plane of phragmoplasts between sets of separating daughter chromosomes during cytokinesis (**Fig. 7E**).

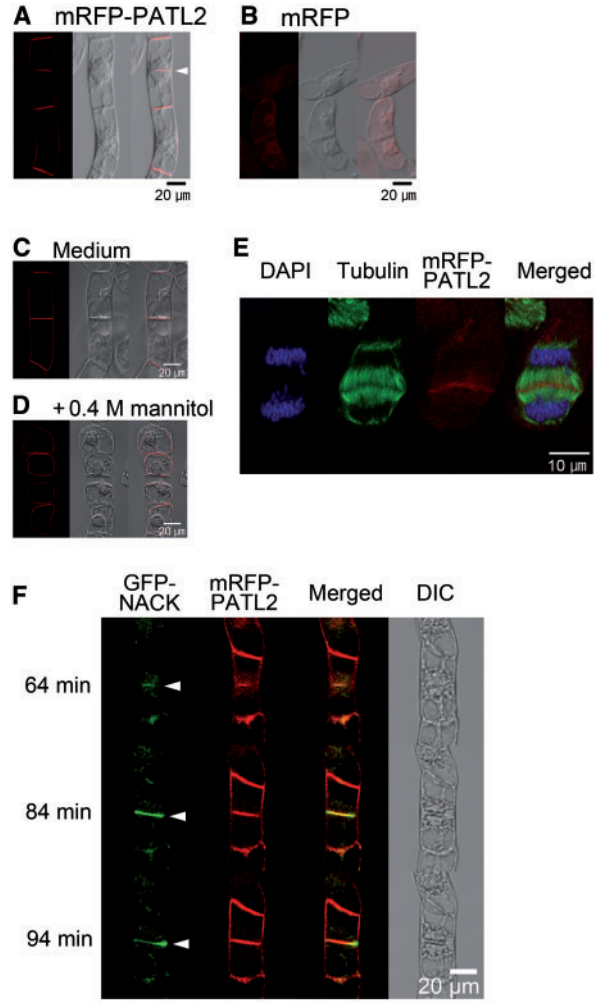

Fig. 7 Intracellular localization of PATL2 in tobacco BY-2 cells. (A) Tobacco BY-2 cells expressing mRFP–PATL2. The developing cell plate in the dividing cell is indicated by an arrowhead. (B) Tobacco BY-2 cells expressing mRFP. (C, D) Tobacco BY-2 cells that expressed mRFP–PATL2 were incubated without (C) and with (D) 0.4 M mannitol. The high concentration of mannitol caused plasmolysis. (A–D) The left, center and right panels show fluorescence due to mRFP, the differential interference contrast (DIC) image and the merged image, respectively. (E) Immunofluorescence staining, at telophase, of microtubules in a tobacco BY-2 cell that expressed mRFP–PATL2. Blue, green and red indicate signals due to 4′,6-diamidino-2-phenylindole (DAPI), α-tubulin and mRFP, respectively. (F) Time-course analysis of the localization of mRFP–PATL2 and GFP-fused NACK1 in BY-2 cells. Transformed cells were cultured in synchrony from prometaphase by two-step synchronization with aphidicolin and propyzamide. The fluorescence due to GFP-fused NACK1 and that due to PATL2 is represented by green and red coloration, respectively. The arrowheads indicate equatorial planes of cell division. The time (minutes) after the release from inhibition of progression of the cell cycle by propyzamide is indicated. DIC images are shown on the right. The video image is shown in **Supplementary Movie S1**.

We examined the localization of fluorescence signals due to both mRFP–PATL2 and GFP-fused NACK1 (GFP–NACK1) during cytokinesis in living BY-2 cells by time-lapse imaging. We transformed BY-2 cells with DNA constructs for these fusion proteins and synchronized the cell cycle of the

transformed cells at prometaphase by two-step synchronization with aphidicolin and propyzamide as described in the Materials and Methods. During culturing of the cells after removal of promyzamide, signals due to the two fluorescent proteins were almost co-localized during the progression of cytokinesis (64, 84 and 94 min after the removal of propyzamide; **Fig. 7F**; **Supplementary Movie S1**). The respective intensities of the signals due to the two fluorochromes at the cell plate appeared to be similar at 64 and 84 min. Differences in the patterns of signals due to RFP and GFP became apparent at 94 min: the signal due to mRFP–PATL2 was distributed uniformly over the cell plate at 94 min, while the signal due to GFP–NACK1 was more intense at the periphery of the cell plate than in the internal region, an observation consistent with the previous result (Nishihama et al. 2002). These observations supported our hypothesis that PATL2 is temporarily retained at the division plane after the maturation of the cell plate.

PATL2 binds to phosphoinositides and its binding activity is affected by phosphorylation by MPK4

We examined the ability of recombinant PATL2 to bind phosphoinositides by a protein–lipid overlay assay. Maltose-binding protein-fused PATL2 (MBP–PATL2) that had been synthesized in *E. coli* was purified, and tested for binding to various phosphoinositides that had been immobilized onto nitrocellulose membranes. The MBP–PATL2 that had bound to phosphoinositides was visualized by immunostaining with PATL2-specific antibodies (**Fig. 8A**). Although MBP–PATL2 did not bind to phosphatidylinositol (PI), it bound to all seven phosphorylated forms of PI: phosphatidylinositol monophosphates (PIPs: PI3P; PI4P; PI5P), phosphatidylinositol bisphosphates [PIP_2: $PI(3,4)P_2$; $PI(3,5)P_2$; $PI(4,5)P_2$] and phosphatidylinositol 3,4,5-triphosphate [$PI(3,4,5)P_3$] (**Fig. 8A**). The binding affinity for PIP was higher than that for PIP_2, which was higher than that for $PI(3,4,5)P_3$.

We examined whether phosphorylation of PATL2 by MPK4 might have an effect on the binding activity of PATL2 to phosphoinositides since the mutated residue at position 536 was located near the SEC14 lipid-binding domain (**Fig. 2A**). MBP–PATL2 was phosphorylated by MPK4 in vitro with [γ-^{32}P]ATP and subjected to protein–lipid overlay assays. MBP–PATL2 that bound to phosphoinositides was visualized by autoradiography. As shown in **Fig. 8B**, the binding patterns of phosphorylated PATL2 to phosphoinositides were altered by the phosphorylation: the affinity of phosphorylated PATL2 for PIP was relatively reduced. In contrast, the affinity of phosphorylated PATL2 for PIP_2 and that for $PI3,4,5P_3$ were relatively increased. These results suggest that phosphorylation by MPK4 altered the binding activity of PATL2 depending on the extent of phosphorylation of phosphoinositides.

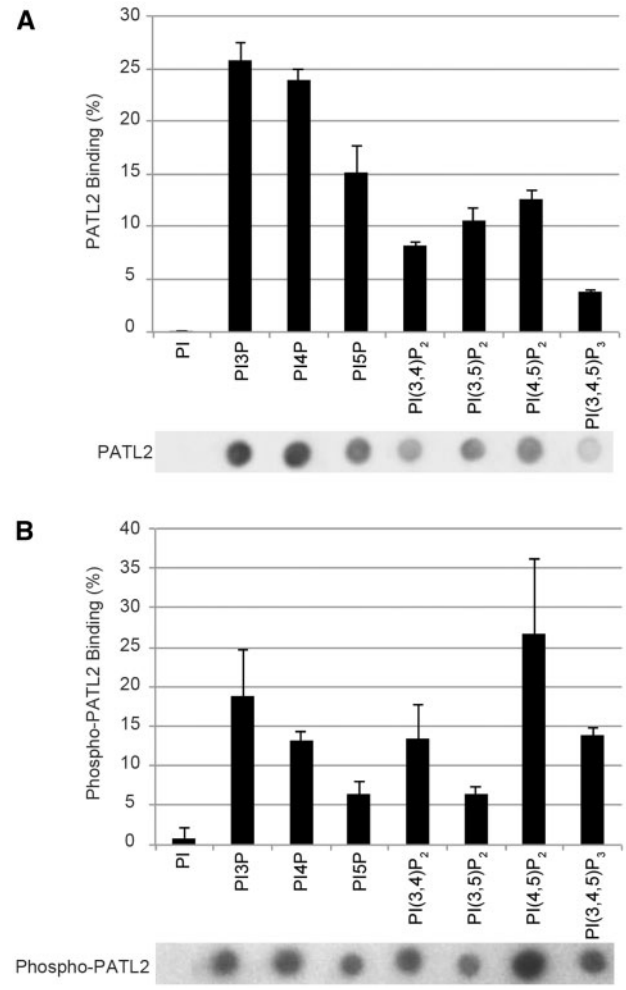

Fig. 8 Phosphoinositide binding properties of PATL2 and phosphorylated PATL2. (A) Relative binding activity of PATL2. MBP–PATL2 was subjected to the protein–lipid overlay assay with the indicated phosphoinositides, and MBP–PATL2 bound to the membrane was detected with PATL2-specific antibodies, which was visualized with horseradish peroxidase-conjugated goat anti-rabbit IgG antibodies as described in the Materials and Methods (lower panel). The intensities of signals due to MBP–PATL2 were determined with ImageJ (http://imagej.nih.gov/ij/) after immunochemical detection. The percentage of the MBP–PATL2 intensity bound in each spot was calculated against the total signals of all spots (upper panel). Values are the means ± SD from three replicate experiments. (B) Relative binding activity of MPK4-phosphorylated PATL2. MBP–PATL2 protein was labeled with [γ-^{32}P]ATP by MPK4, and the labeled protein was subjected to the protein–lipid overlay assay as described in the Materials and Methods. Radioactivity was detected by autoradiography (lower panel). The intensities of radioactive spots were determined as described above. The percentage of the intensity in each spot was calculated against the total radioactivity of all spots (upper panel). Values are the means ± SD of four replicate experiments.

Discussion

The SEC14-domain protein PATL2 is phosphorylated by MPK4 MAP kinase

The present study showed that comparative phosphoproteomics, with proteins prepared from wild-type and *mpk4* plants, by 2D-DIGE is an effective initial screening technique for identification of protein substrates of MPK4 MAP kinase that is required for formation of the cell plate. Exploiting this technique, we found that the SEC14 domain protein PATL2 is phosphorylated by MPK4 both in vivo and in vitro (**Figs. 1**, **2**, **4**, **5**).

We also showed that GFP–PATL2 is concentrated at the site of formation of the cell plate in the phragmoplast of dividing cells, where MPK4 is similarly concentrated in dividing cells (Kosetsu et al. 2010), and at the cell periphery in non-dividing cells, in which the GFP–PATL2 proteins are concentrated at plasma membranes (**Figs. 6**, **7**). PATL2 binds to all seven phosphorylated forms of PI, but not to PI itself, and phosphorylation of PATL2 by MPK4 alters the binding affinity among the phosphoinositides. These results suggest a role for the PATL2 protein downstream of MPK4 in formation of the cell plate, including the regeneration of membranes during cytokinesis. The role of phosphorylation of PATL2 by MPK4 in cytokinesis should, however, be further investigated since the relevance of the alteration of binding properties of phosphorylated PATL2 to phosphoinositides is still not known.

PATL2 belongs to the PATL protein family, which consists of six members in *A. thaliana*, and is characterized by two previously defined domains: a SEC14 domain and a Golgi dynamics (GOLD) domain (Peterman et al. 2004). MPK4 MAP kinase phosphorylates the serine residue at position 536 in the SEC14 domain that is ubiquitously conserved in all eukaryotes examined (**Figs. 2**, **5**). Potential phosphorylation of this serine residue was reported by Durek et al. (2010). The SEC14 domain has the ability to bind to several specific phosphoinositides and to transfer these molecules from one membrane component to another (Routt and Bankaitis 2004, Saito et al. 2007, Schaaf et al. 2008, Bankitis et al. 2010, LeBlanc and McMaster 2010). The GOLD domain is involved in protein–protein interactions with a number of proteins that are related to Golgi function and vesicle traffic (Anantharaman and Aravind 2002, Montesinos et al. 2014). The phosphorylatable serine residue at position 536 of PATL2 is present in the lipid-binding pocket (Sha et al. 1998, Sha and Luo 1999, Peterman et al. 2004), which is immediately adjacent to amino acid residues that are involved in the transfer of phosphoinositides (Cleves et al. 1989, Li et al. 2000). These observations are consistent with our present result that PATL2 might participate in the membrane regeneration that is associated with formation of the cell plate during cytokinesis.

Functions of other SEC14-domain proteins in plants

Although many SEC14-related proteins have been found in plants, the roles of only two of them have been elucidated. Nlj16-like nodulin (a nodule-specific protein) is a member of the nodulin family and was first identified in *Lotus japonicus*. It is characterized by the SEC14 domain that is followed by the nodulin domain (Kapranov et al. 2001). The genome of *A. thaliana* encodes 13 genes for SEC14-nodulin proteins (Böhm et al. 2004, Vincent et al. 2005). Many such genes are expressed predominantly in cells that exhibit extremely polarized membrane growth, such as pollen cells and root hair cells. For example, the *COW* (*can of worms1*) gene (allelic to *SRH1* and *AtSFH1*, a SEC14 homolog in *A. thaliana*) is essential for the polarized expansion of cells in root hairs (Böhme et al. 2004, Vincent et al. 2005, Ghosh et al. 2015).

Expression of another member of the SEC14-gene superfamily in *Nicotiana benthamiana* (*NbSEC14*) is induced in response to infection with the plant pathogenic bacterium *Ralstonia solanacearum*, and development of disease and bacterial growth were shown to be accelerated in *NbSEC14*-silenced plants (Kiba et al. 2012). Moreover, evidence for a correlation between phospholipid metabolism and plant immune responses that involves NbSEC14 has also been reported (Kiba et al. 2014).

PATL2 is different in terms of phosphorylation of their proteins and the binding affinity for phosphoinositides from PATL1

The results of in vivo and in vitro experiments in the present study (**Figs. 1**, **2**, **4**, 5) suggest that a majority of PATL2 proteins are phosphorylated at a single residue and that some PATL2 proteins are phosphorylated at two residues at least (**Fig. 4**). These residues may include the serine residue at position 536 that is phosphorylated by MPK4 (**Figs. 4**, **5**). Two previous phosphoproteomic analyses (Hsu et al. 2009, Nakagami et al. 2010, Černý et al. 2011) indicated that PATL2 is phosphorylated in two other regions, which differ from the sites of phosphorylation that we identified: these former phosphorylation events are induced in response to treatment with salts and cytokinin, respectively, suggesting potential links between phosphorylation of PATL2 and cellular responses to these treatments. According to Durek et al. (2010), 11 peptide regions of PATL2, including the three regions described above, are putative sites of phosphorylation. Thus, PATL2 is a multiply phosphorylated protein. The full complement of protein kinases that phosphorylate these sites remains to be identified.

PATL1, the closest known homolog of PATL2, is suggested to play a role in membrane trafficking events during the maturation stage of plant cytokinesis because of its concentration pattern at recently matured cell plates and its phosphoinositide-binding properties (Peterman et al. 2004). Although PATL1 and PATL2 have strongly conserved amino acid sequences, which are 88% and 75% identical in the SEC14 and GOLD domains, respectively, they do not share any phosphorylation sites in these domains (Durek et al. 2010). The phosphorylation of PATL1 by a protein kinase remains, however, to be demonstrated. The binding properties of PATL1 to phosphoinositides are also distinct from those of PATL2: PATL1 binds to PI and several phosphorylated forms, but has no affinity for PI(3,4)P_2 (Peterman et al. 2004). In contrast, PATL2 binds to all seven phosphoinositides but has no affinity for PI (**Fig. 8A**).

PATL1 and PATL2 might each be integrated separately into a distinct regulatory network and each might be controlled differently by phosphorylation. Nevertheless, both proteins are localized at cell plates during cytokinesis and their accumulation within cells is affected similarly by treatment with brassinosteroids (Deng et al. 2007), suggesting the possible involvement of these two proteins in similar cellular processes. With respect to the distinct roles of these two PATLs, it is worth noting that they have different subcellular localizations in interphase cells. Immunolocalization showed that PATL1 is localized in a punctate pattern in Golgi-like structures in the cytoplasm (Peterman et al. 2004), while our analyses of GFP- and RFP-fused PATL2 revealed fluorescent signals at the plasma

membranes at the cell periphery (Fig. 7). The different patterns of subcellular localization might reflect distinct temporal patterns of phosphorylation of the two PATLs.

In the preliminary experiments, we found that the *patl1 patl2* double mutant has no obvious cytokinetic defects (our unpublished result). Other members of the PATL protein family might act redundantly with respect to PATL1 and PATL2 in cytokinesis. PATL3 and PATL6 have been reported to interact with virus-movement protein at plasmodesmata (Peiro et al. 2014), and primary plasmodesmata are, in fact, formed at cytokinesis (Zambryski 1995). The roles of members of the PATL family during cytokinesis merit further investigation.

In conclusion, we have identified the SEC14–GOLD-domain protein PATL2 as a substrate of MPK4 MAP kinase that is required for formation of the cell plate. MPK4 phophorylates the single serine residue at position 536 in PATL2 protein in the lipid-binding pocket of its SEC14 domain. PATL2 is concentrated at the cell division plane where MPK4 is localized in dividing cells as well as at the plasma membrane in interphase cells. The binding properties of PATL2 to phosphoinositides were altered after phosphorylation of PATL2 by MPK4. These results suggest a role for the MAPK–PATL2 pathway in the regeneration of membranes during cytokinesis. MPK4 also phosphorylates some members of the MAP65 family, which stimulates turnover of MTs that enhances centrifugal expansion of the phragmoplast (Sasabe et al. 2006, Beck et al. 2010, Kosetsu et al. 2010, Sasabe et al. 2011b). MPK4 might be involved in at least two molecular processes for plant cytokinesis: the turnover of MTs and the regeneration of cell membranes.

Materials and Methods

Extraction and purification of phosphorylated proteins from roots

The protocol for the phenol extraction of proteins was a modified version of that described elsewhere (Hurkman and Tanaka 1986). The roots of 10-day-old wild-type and mutant plants of *A. thaliana*, grown on vertical plates, were ground in liquid nitrogen with a pestle and mortar . Each resultant powder was suspended in 10 vols. of extraction buffer [0.5 M Tris–HCl, pH 7.5; 0.7 M sucrose, 50 mM EDTA, 0.1 M KCl, 2 mM phenylmethylsulfonyl fluoride (PMSF) and 20 mM dithiothreitol] and then an identical volume of Tris-saturated phenol was added with vigorous mixing. The solution was centrifuged and the phenol phase was collected. After the addition of extraction buffer and centrifugation, the proteins in the phenol phase were precipitated with 5 vols. of methanol at −20°C for >2 h. The precipitated proteins were washed with cold acetone, dried, and then dissolved in swelling buffer (7 M urea, 2 M thiourea and 4% CHAPS). To obtain a fraction enriched for phosphorylated proteins, the extracted proteins were treated with a PhosphoProtein Purification kit (Qiagen; http://www.qiagen.com/).

2D-DIGE

Proteins in phosphoprotein-enriched fractions were precipitated with a 2-D Clean-Up kit (GE Healthcare; http://www.gelifesciences.com/). Precipitates were dissolved in three equal volumes of precipitant buffer provided by the manufacturer, and the mixture was put on ice for 15 min. The precipitate was recovered by centrifugation and dissolved in the same volume of co-precipitant, and the precipitate was again recovered by centrifugation. The precipitate was dissolved in 25 μl of water, and 1 ml of wash buffer and 5 μl of wash additive were added to the sample. After incubation at −20°C for 30 min, the precipitate was recovered, air-dried and dissolved in buffer that contained 30 mM Tris–HCl (pH 8.5), 2 M thiourea, 7 M urea and 4% CHAPS. Phosphorylated proteins were labeled with the CyDye™ DIGE Fluor Minimal Labeling kit (GE Healthcare) with Cy2, Cy3 or Cy5 according to the manufacturer's protocol: 400 pmol of dye was added to 50 μg of protein in the above buffer and the mixture was kept on ice for 30 min. A mixture of labeled proteins from wild-type and mutant plants was then subjected to isoelectric focusing with Immobiline™ DryStrip and Ettan IPGphor II (GE Healthcare). After subsequent SDS–PAGE, protein spots were visualized with the Typhoon system (GE Healthcare), and the intensity of each spot was determined with DeCyder software (GE Healthcare).

Identification of proteins

A 500 μg aliquot of a phosphoprotein-enriched fraction of proteins from roots of 10-day-old wild-type plants were fractionated by isoelectric focusing and SDS–PAGE as described above. Gels were stained with Deep Purple™ (GE Healthcare). Spots of interest were excised with an Ettan Spot Picker (GE Healthcare), digested with trypsin in situ, and then analyzed by MALDI-TOF/MS with a Voyager system (Applied Biosystems; http://www.appliedbiosystems.com/).

Production of antibodies and immunodetection of proteins

Antibodies against PATL2 were raised by immunizing rabbits with the synthetic peptide CDDLVSEDLEGSEFC (residues 399–411 of PALT2), which was synthesized and affinity-purified by MBL (http://www.mbl.co.jp/). The protein extracts (10 μg) were subjected to SDS–PAGE (8% acrylamide, 0.21% bis-acrylamide). For 2D-Western blotting, protein extracts (50 μg) were subjected to isoelectric focusing followed by SDS–PAGE. Blotting and immunodetection were performed as described previously by Nishihama et al. (2001). Signals were detected with SuperSignal™ West Femto Maximum Sensitivity Substrate (Thermo Scientific, http://www.thermoscientific.com/) and LAS-4000 mini (GE Healthcare). For detection of PATL2, we used specific affinity-purified antibodies at a concentration of 0.31 μg ml^{-1}.

Real-time RT–PCR

The protocol for real-time RT–PCR was a modified version of that described previously (Kojima et al. 2011). Roots of wild-type and mutant plants were harvested 10 d after sowing and frozen immediately in liquid nitrogen. Total RNA was isolated with the High Pure RNA Tissue kit (Roche, http://roche-biochem.com/). For the analysis of levels of RNAs by real-time PCR, we prepared 50 ng of total RNA for conversion to cDNA using ReverTra Ace® (Toyobo, http://www.toyobo.co.jp/). PCR was performed using a SYBR® Green II kit (TAKARA, http://www.takara-bio.co.jp/) with primer pairs as follows: for PATL2, 5′-CCAGAGTTTGTCGCTAAAGAGC-3′ and 5′-TGTCCTTGGCGATGTAATGA-3′; and for eIF5A, 5′-CGTGTTGATTACCAGTTGATTGA-3′ and 5′-TGGGAAGCTTGAGATCATCC-3′. Amplification was monitored in real time with the Thermal Cycler Dice® Real Time System II (TAKARA), according to the supplier's recommendations.

Fluorescence microscopy and synchronization of cells

All techniques for microscopic analysis were described previously (Nishihama et al. 2001). Fluorescence was observed with an LSM510 (Carl Zeiss, http://www.zeiss.com/) and FV1000 (Olympus, http://www.olympus.co.jp/) confocal microscope. Synchronization of the cell cycle was performed basically as described by Nagata and Kumagai (1999). Cells were cultured for 24 h in medium that contained 5 mg l^{-1} aphidicolin (Wako) and washed with fresh medium without aphidicolin. Cells were then cultured in medium that contained 3 μM propyzamide (Wako) for 4 h and examined after washing with fresh medium without propyzamide.

Kinase assay in vitro

To obtain active MPK4, we incubated 100 ng of recombinant HisT7-MPK4 and 150 ng of GST–NQK1 in kinase buffer (Nishihama et al. 2001) that contained

500 μM ATP for 60 min at 25°C. A 1 μg aliquot of tag-fused PATL2 and 10 μCi of [γ-^{32}P]ATP were added to the reaction mixture, which was then incubated for a further 30 min. The kinase reaction was stopped by addition of sample buffer for SDS–PAGE and products were separated by SDS–PAGE. Phosphorylated proteins were detected by autoradiography.

A. thaliana mutants

The PATL2 and PATL1 mutants were obtained from the ABRC (https://abrc.osu.edu/). SALK_009982, SALK_075774, SALK_086866, SALK_103668 and SALK_080204 were renamed *patl2-1*, *patl2-2*, *patl2-3*, *patl1-2* and *patl1-2*, respectively. Pairs, namely *patl2-1*/*patl1-2* and *patl2-3*/*patl1-2*, were crossed to generate double mutants, which were confirmed by identifying sites of insertion of the T-DNAs by PCR analysis.

Construction of plasmids

The cDNA for PATL2 was cloned by RT–PCR with primers 5′-ACAAGTTTGTACAAAAAAGCAGGCTTCATGGCTCAAGAAGAGATACAG-3′ and 5′-ACCACTTTGTACAAGAAAGCTGGGTATGCTTGGGTTTTGGACCT-3′. The amplified DNA fragment was cloned into pDONR201 with BP clonase® (Life Technologies, http://www.lifetechnologies.com/). From this entry clone, the recombinant cDNA was transferred to various destination vectors by LR® clonase (Life Technologies). For expression of GST-fused and MBP-fused PATL2 in *E. coli*, pDEST17 and pDESTMAL, derived from pMAL-c5X, were used as destination vectors, respectively. Two types of fluorescent proteins were fused to PATL2: G3GFP, which has two amino acid substitutions (Ser65 and Tyr145) with alanine and phenylalanine, respectively (Kawakami and Watanabe 1997), and mRFP. For expression of these fusion genes, a series of pGWB plasmids was used as destination vectors (Nakagawa et al. 2007). The binary vectors were introduced into plants by *Agrobacterium*-mediated transformation.

Protein–lipid overlay assay

To assess the phosphoinositide-binding properties of PATL2, a protein–lipid overlay assay was performed by using MBP–PATL2, as described previously (Dowler et al. 2000). PI and PI3,4,5P_3 were purchased from Sigma-Aldrich. PI3P, PI4P, PI5P, PI3,4P_2, PI3,5P_2 and PI4,5P_2 were purchased from Wako Pure Chemical. A lipid solution (1 μl) containing 0.25 nmol phosphoinositides dissolved in a mixture of chloroform/methanol/water (1 : 2 : 0.8, by vol.) was spotted onto a Hybond-C extra membrane. The membrane was blocked in 3% (w/v) fatty acid-free bovine serum albumin (BSA) in TBST [50 mM Tris–HCl, pH 7.5, 150 mM NaCl and 0.1% (v/v) Tween-20] for 1 h. The membrane was then incubated overnight at 4°C with gentle stirring in the same solution containing 10 μg ml^{-1} MBP–PATL2. The membranes were washed six times over 30 min in TBST and then incubated for 1 h with a 1 : 1,000 dilution of anti-PATL2-specific antibodies. The membranes were washed as before, then incubated for 1 h with a 1 : 5,000 dilution of horseradish peroxidase-conjugated goat anti-rabbit IgG antibodies. Finally, the membranes were washed 12 times over 1 h in TBST, and the MBP–PATL2 protein that was bound to the membrane by virtue of its interaction with phospholipid was detected by enhanced chemiluminescence. Signal intensities were determined with ImageJ (http://imagej.nih.gov/ij/). Recombinant MBP–PATL2 protein was phosphorylated by activated HisT7-MPK4 in the presence of [γ-^{32}P]ATP. After a 30 min incubation at 25°C, MBP–PATL2 was purified with amylose resin (New England BioLabs, http://www.neb.com/). The protein–lipid overlay assay with labeled MBP–PATL2 was performed as described above.

Supplementary data

Supplementary data are available at PCP online.

Funding

This work was supported by the Program for the Promotion of Basic Research Activities for Innovative Biosciences (BRAIN) [a grant to Y.M. and a grant to T.S.]; the Ministry of Education, Culture, Sports, Science and Technology of Japan [a Grant-in-Aid for Scientific Research on Priority Areas (No. 19060003 to Y.M.) and a grant from the Global COE Program 'Advanced Systems-Biology']; the Japan Society for the Promotion of Science [a Grant-in-Aid for Scientific Research (B) (No. 23370021 to Y.M.)].

Disclosures

The authors have no conflicts of interest to declare.

Acknowledgments

The authors thank Dr. H. Kosako for his encouragement and helpful comments; Drs. Y. Yoshioka, and Y. Ueno for helpful discussions and technical assistance; Dr. K. Nakamura and other members of his laboratory for helpful discussions; and Ms. T. Shinagawa for her skilled technical assistance.

References

Anantharaman, V. and Aravind, L. (2002) The GOLD domain, a novel protein module involved in Golgi function and secretion. *Genome Biol.* 3: research0023.

Bankaitis, V.A., Mousley, C.J. and Schaaf, G. (2010) The Sec14 superfamily and mechanisms for crosstalk between lipid metabolism and lipid signaling. *Trends Biochem. Sci.* 35: 150–160.

Beck, M., Komis, G., Müller, J., Menzel, D. and Samaj, J. (2010) *Arabidopsis* homologs of nucleus- and phragmoplast-localized kinase 2 and 3 and mitogen-activated protein kinase 4 are essential for microtubule organization. *Plant Cell* 22: 755–771.

Betsuyaku, S., Takahashi, F., Kinoshita, A., Miwa, H., Shinozaki, K., Fukuda, H., et al. (2011) Mitogen-activated protein kinase regulated by the CLAVATA receptors contributes to shoot apical meristem homeostasis. *Plant Cell Physiol.* 52: 14–29.

Böhme, K., Li, Y., Charlot, F., Grierson, C., Marrocco, K., Okada, K., Laloue, M., et al. (2004) The *Arabidopsis COW1* gene encodes a phosphatidylinositol transfer protein essential for root hair tip growth. *Plant J.* 40: 686–698.

Boutté, Y., Frescatada-Rosa, M., Men, S., Chow, C.M., Ebine, K., Gustavsson, A., et al. (2010) Endocytosis restricts *Arabidopsis* KNOLLE syntaxin to the cell division plane during late cytokinesis. *EMBO J.* 29: 546–558.

Campbell, R.E., Tour, O., Palmer, A.E., Steinbach, P.A., Baird, G.S., Zacharias, D.A., et al. (2002) A monomeric red fluorescent protein. *Proc. Natl. Acad. Sci. USA* 99: 7877–7882.

Cargnello. M. and Roux, P.P. (2011) Activation and function of the MAPKs and their substrates, the MAPK-activated protein kinases. *Microbiol. Mol. Biol. Rev.* 75: 50–83.

Černý, M., Dyčka, F., Bobálová, J. and Brzobohatý, B. (2011) Early cytokinin response proteins and phosphoproteins of *Arabidopsis thaliana* identified by proteome and phosphoproteome profiling. *J. Exp. Bot.* 62: 921–937.

Chang, L. and Karin, M. (2001) Mammalian MAP kinase signalling cascades. *Nature* 410: 37–40.

Cleves, A.E., Novick, P.J. and Bankaitis, V.A. (1989) Mutations in the *SAC1* gene suppress defects in yeast Golgi and yeast actin function. *J. Cell Biol.* 109: 2939–2950.

Deng, Z., Zhang, X., Tang, W., Oses-Prieto, J.A., Suzuki, N., Gendron, J.M., et al. (2007) A proteomics study of brassinosteroid response in *Arabidopsis*. *Mol. Cell Proteomics* 6: 2058–2071.

Dowler, S., Currie, R.A., Campbell, D.G., Deak, M., Kular, G., Downes, C.P., et al. (2000) Identification of pleckstrin-homology-domain-containing proteins with novel phosphoinositide-binding specificities. *Biochem. J.* 351: 19–31.

Durek, P., Schmidt, R., Heazlewood, J.L., Jones, A., MacLean, D., Nagel, A., et al. (2010) PhosPhAt: the *Arabidopsis thaliana* phosphorylation site database. An update. *Nucleic Acids Res.* 38: D828–D834.

Frescatada-Rosa, M., Stanislas, T., Backues, S.K., Reichardt, I., Men, S., Boutté, Y., et al. (2014) High lipid order of *Arabidopsis* cell-plate membranes mediated by sterol and DYNAMIN-RELATED PROTEIN1A function. *Plant J.* 80: 745–757.

Ghosh, R., de Campos, M.K., Huang, J., Huh, S.K., Orlowski, A., Yang, Y., et al. (2015) Sec14-nodulin proteins and the patterning of phosphoinositide landmarks for developmental control of membrane morphogenesis in *Arabidopsis*. *Mol. Biol. Cell.* 26: 1764–1781.

Heese, M., Mayer, U. and Jürgens, G. (1998) Cytokinesis in flowering plants: cellular process and developmental integration. *Curr. Opin. Plant Biol.* 1: 486–491.

Hsu, J.L., Wang, L.Y., Wang, S.Y., Lin, C.H., Ho, K.C., Shi, F.K., et al. (2009) Functional phosphoproteomic profiling of phosphorylation sites in membrane fractions of salt-stressed *Arabidopsis thaliana*. *Proteome Sci.* 7: 42.

Hurkman, W.J. and Tanaka, C.K. (1986) Solubilization of plant membrane proteins for analysis by two-dimensional gel electrophoresis. *Plant Physiol.* 81: 802–806.

Ishikawa, M., Soyano, T., Nishihama, R. and Machida, Y. (2002) The NPK1 mitogen-activated protein kinase kinase kinase contains a functional nuclear localization signal at the binding site for the NACK1 kinesin-like protein. *Plant J.* 32: 789–798.

Kapranov, P., Routt, S.M., Bankaitis, V.A., de Bruijn, F.J. and Szczyglowski, K. (2001) Nodule-specific regulation of phosphatidylinositol transfer protein expression in *Lotus japonicus*. *Plant Cell* 13: 1369–1382.

Kawakami, S. and Watanabe, Y. (1997) Use of green fluorescent protein as a molecular tag of protein movement in vivo. *Plant Biotechnol.* 14: 127–130.

Kiba, A., Galis, I., Hojo, Y., Ohnishi, K., Yoshioka. H. and Hikichi, Y. (2014) SEC14 phospholipid transfer protein is involved in lipid signaling-mediated plant immune responses in *Nicotiana benthamiana*. *PLoS One* 9: e98150.

Kiba, A., Nakano, M., Vincent-Pope, P., Takahashi, H., Sawasaki, T., Endo, Y., et al. (2012) A novel Sec14 phospholipid-transfer protein from *Nicotiana benthamiana* is upregulated in response to *Ralstonia solanacearum* infection, pathogen-associated molecular patterns and effector molecules and involved in plant immunity. *J. Plant Physiol.* 169: 1017–1022.

Kojima, S., Iwasaki, M., Takahashi, H., Imai, T., Matsumura, Y., Fleury, D., et al. (2011) Asymmetric leaves2 and Elongator, a histone acetyltransferase complex, mediate the establishment of polarity in leaves of *Arabidopsis thaliana*. *Plant Cell Physiol.* 52: 1259–1273.

Kong, Q., Qu, N., Gao, M., Zhang, Z., Ding, X., Yang, F., et al. (2012) The MEKK1–MKK1/MKK2–MPK4 kinase cascade negatively regulates immunity mediated by a mitogen-activated protein kinase kinase kinase in *Arabidopsis*. *Plant Cell* 24: 2225–2236.

Kosetsu, K., Matsunaga, S., Nakagami, H., Colcombet, J., Sasabe, M., Soyano, T., et al. (2010) The MAP kinase MPK4 is required for cytokinesis in *Arabidopsis thaliana*. *Plant Cell* 22: 3778–3790.

Lampard, G.R., MacAlister, C.A. and Bergmann, D.C. (2008) *Arabidopsis* stomatal initiation is controlled by MAPK-mediated regulation of the bHLH SPEECHLESS. *Science* 322: 1113–1116.

LeBlanc, M.A. and McMaster, C.R. (2010) Surprising roles for phospholipid-binding proteins revealed by high-throughput genetics. *Biochem. Cell Biol.* 88: 565–574.

Li, X., Xie, Z. and Bankaitis V.A. (2000) Phosphatidylinositol/phosphatidylcholine-transfer proteins in yeast. *Biochim. Biophys. Acta* 1486: 55–71.

Meng, X. and Zhang, S. (2013) MAPK cascades in plant disease resistance signaling. *Annu. Rev. Phytopathol.* 51: 245–266.

Montesinos, J.C., Pastor-Cantizano, N., Robinson, D.G., Marcote, M.J. and Aniento, F. (2014) *Arabidopsis* p24δ5 and p24δ9 facilitate coat protein I-dependent transport of the K/HDEL receptor ERD2 from the Golgi to the endoplasmic reticulum. *Plant J.* 80: 1014–1030.

Mousley, C.J., Tyeryar. K.R., Vincent-Pope, P. and Bankaitis, V.A. (2007) The Sec14-superfamily and the regulatory interface between phospholipid metabolism and membrane trafficking. *Biochim. Biophys. Acta* 1771: 727–736.

Murata, T., Sano, T., Sasabe, M., Nonaka, S., Higashiyama, T., Hasezawa, S., et al. (2013) Mechanism of microtubule array expansion in the cytokinetic phragmoplast. *Nat.Commun.* 4: 1967.

Nagata, T. and Kumagai, F. (1999) Plant cell biology through the window of the highly synchronized tobacco BY-2 cell line. *Methods Cell Sci.* 21: 123–127.

Nakagami, H., Pitzschke, A. and Hirt, H. (2005) Emerging MAP kinase pathways in plant stress signalling. *Trends Plant Sci.* 10: 339–346.

Nakagami, H., Sugiyama, N., Mochida, K., Daudi, A., Yoshida, Y., Toyoda, T., et al. (2010) Large-scale comparative phosphoproteomics identifies conserved phosphorylation sites in plants. *Plant Physiol.* 153: 1161–1174.

Nakagawa, T., Suzuki, T., Murata, S., Nakamura, S., Hino, T., Maeo, K., et al. (2007) Improved gateway binary vectors: high-performance vectors for creation of fusion constructs in transgenic analysis of plants. *Biosci. Biotechnol. Biochem.* 71: 2095–2100.

Naito, H. and Goshima, G. (2015) NACK kinesin is required for metaphase chromosome alignment and cytokinesis in the moss *Physcomitrella patens*. *Cell Struct. Funct.* 40: 31–41.

Nishihama, R., Ishikawa, M., Araki, S., Soyano, T., Asada, T. and Machida, Y. (2001) The NPK1 mitogen-activated protein kinase kinase kinase is a regulator of cell-plate formation in plant cytokinesis. *Genes Dev.* 15: 352–363.

Nishihama, R. and Machida, Y. (2001) Expansion of the phragmoplast during plant cytokinesis: a MAPK pathway may MAP it out. *Curr. Opin. Plant Biol.* 4: 507–512.

Nishihama, R., Soyano, T., Ishikawa, M., Araki, S., Tanaka, H., Asada, T., et al. (2002) Expansion of the cell plate in plant cytokinesis requires a kinesin-like protein/MAPKKK complex. *Cell* 109: 87–99.

Otegui, M.S. and Staehelin, L.A. (2000) Cytokinesis in flowering plants: more than one way to divide a cell. *Curr. Opin. Plant Biol.* 3: 493–502.

Otegui, M.S., Verbrugghe, K.J. and Skop, A.R. (2005) Midbodies and phragmoplasts: analogous structures involved in cytokinesis. *Trends Cell Biol.* 15: 404–413.

Peiro, A., Izquierdo-Garcia, A.C., Sanchez-Navarro, J.A., Pallas, V., Mulet, J.M. and Aparicio, F. (2014) Patellins 3 and 6, two members of the plant Patellin family, interact with the movement protein of Alfalfa mosaic virus and interfere with viral movement. *Mol. Plant Pathol.* 15: 881–891.

Peterman, T.K., Ohol, Y.M., McReynolds, L.J. and Luna, E.J. (2004) Patellin1, a novel Sec14-like protein, localizes to the cell plate and binds phosphoinositides. *Plant Physiol.* 136: 3080–3094.

Petersen, M., Brodersen, P., Naested, H., Andreasson, E., Lindhart, U., Johansen, B., et al. (2000) *Arabidopsis* MAP kinase 4 negatively regulates systemic acquired resistance. *Cell* 103: 1111–1120.

Routt, S.M. and Bankaitis, V.A. (2004) Biological functions of phosphatidylinositol transfer proteins. *Biochem. Cell Biol.* 82: 254–262.

Saito, K., Tautz, L. and Mustelin, T. (2007) The lipid-binding SEC14 domain. *Biochim. Biophys. Acta* 1771: 719–726.

Sasabe, M., Boudolf, V., De Veylder, L., Inzé, D., Genschik, P. and Machida, Y. (2011a) Phosphorylation of a mitotic kinesin-like protein and a MAPKKK by cyclin-dependent kinases (CDKs) is involved in the transition to cytokinesis in plants. *Proc. Natl. Acad. Sci. USA* 108: 17844–17849.

Sasabe, M., Ishibashi, N., Haruta, T., Minami, A., Kurihara, D., Higashiyama, T. et al. (2015) The carboxyl-terminal tail of the stalk of *Arabidopsis*

NACK1/HINKEL kinesin is required for its localization to the cell-plate formation site. *J. Plant Res.* 128: 327–336.

Sasabe, M., Kosetsu, K., Hidaka, M., Murase, A. and Machida, Y. (2011b) *Arabidopsis thaliana* MAP65-1 and MAP65-2 function redundantly with MAP65-3/PLEIADE in cytokinesis downstream of MPK4. *Plant Signal. Behav.* 6: 743–747.

Sasabe, M. and Machida, Y. (2012) Regulation of organization and function of microtubules by the mitogen-activated protein kinase cascade during plant cytokinesis. *Cytoskeleton (Hoboken)* 69: 913–918.

Sasabe M. and Machida Y. (2014) Signaling pathway that controls plant cytokinesis. *Enzymes* 35: 145–165.

Sasabe, M., Soyano, T., Takahashi, Y., Sonobe, S., Igarashi, H., Itoh, T.J., et al. (2006) Phosphorylation of NtMAP65-1 by a MAP kinase down-regulates its activity of microtubule bundling and stimulates progression of cytokinesis of tobacco cells. *Genes Dev.* 20: 1004–1014.

Schaaf, G., Ortlund, E.A., Tyeryar, K.R., Mousley, C.J., Ile, K.E., Garrett, T.A., et al. (2008) Functional anatomy of phospholipid binding and regulation of phosphoinositide homeostasis by proteins of the Sec14 superfamily. *Mol. Cell* 29: 191–206.

Serna L. (2014) The role of brassinosteroids and abscisic acid in stomatal development. *Plant Sci.* 225: 95–101.

Sha, B. and Luo, M. (1999) PI transfer protein: the specific recognition of phospholipids and its functions. *Biochim. Biophys. Acta* 1441: 268–277.

Sha, B., Phillips, S.E., Bankaitis, V.A. and Luo, M. (1998) Crystal structure of the *Saccharomyces cerevisiae* phosphatidylinositol-transfer protein. *Nature* 391: 506–510.

Soyano, T., Nishihama, R., Morikiyo, K., Ishikawa, M. and Machida, Y. (2003) NQK1/NtMEK1 is a MAPKK that acts in the NPK1 MAPKKK-mediated MAPK cascade and is required for plant cytokinesis. *Genes Dev.* 17: 1055–1067.

Strompen, G., El Kasmi, F., Richter, S., Lukowitz, W., Assaad, F.F., Jürgens, G., et al. (2002) The *Arabidopsis HINKEL* gene encodes a kinesin-related protein involved in cytokinesis and is expressed in a cell cycle-dependent manner. *Curr. Biol.* 12: 153–158.

Suzuki, T. and Machida, Y. (2008) MAP kinase cascades controlling cell division, plant growth and development. *Plant Cell Monogr.* 10: 261–275.

Takahashi, Y., Soyano, T., Kosetsu, K., Sasabe, M. and Machida, Y. (2010) HINKEL kinesin, ANP MAPKKKs and MKK6/ANQ MAPKK, which phosphorylates and activates MPK4 MAPK, constitute a pathway that is required for cytokinesis in *Arabidopsis thaliana*. *Plant Cell Physiol.* 51: 1766–1776.

Tanaka, H., Ishikawa, M., Kitamura, S., Takahashi, Y., Soyano, T., Machida, C., et al. (2004) The *AtNACK1/HINKEL* and *STUD/TETRASPORE/AtNACK2* genes, which encode functionally redundant kinesins, are essential for cytokinesis in *Arabidopsis*. *Genes Cells* 9: 1199–1211.

Tang, W., Kim, T.W., Oses-Prieto, J.A., Sun, Y., Deng, Z., Zhu, S., et al. (2008) BSKs mediate signal transduction from the receptor kinase BRI1 in Arabidopsis. *Science* 321: 557–560.

Ueda, K., Kosako, H., Fukui, Y. and Hattori, S. (2004) Proteomic identification of Bcl2-associated athanogene 2 as a novel MAPK-activated protein kinase 2 substrate. *J. Biol. Chem.* 279: 41815–41821.

Vincent, P., Chua, M., Nogue, F., Fairbrother, A., Mekeel, H., Xu, Y., et al. (2005) A Sec14p-nodulin domain phosphatidylinositol-transfer protein polarizes membrane growth of *Arabidopsis thaliana* root hairs. *J. Cell Biol.* 168: 801–812.

Widmann, C., Gibson, S., Jarpe, M.B. and Johnson, G.L. (1999) Mitogen-activated protein kinase: conservation of a three-kinase module from yeast to human. *Physiol. Rev.* 79: 143–180.

Yang, S.H., Sharrocks, A.D. and Whitmarsh, A.J. (2013) MAP kinase signalling cascades and transcriptional regulation. *Gene* 513: 1–13.

Zambryski, P. (1995) Plasmodesmata: plant channels for molecules on the move. *Science* 270: 1943–1944.

Zeng, Q., Chen, J.G. and Ellis, B.E. (2011) AtMPK4 is required for male-specific meiotic cytokinesis in *Arabidopsis*. *Plant J.* 67: 895–906.

Zhang, Z., Wu, Y., Gao, M., Zhang, J., Kong, Q., Liu, Y., et al. (2012) Disruption of PAMP-induced MAP kinase cascade by a *Pseudomonas syringae* effector activates plant immunity mediated by the NB-LRR protein SUMM2. *Cell Host Microbe* 11: 253–263.